Pälike, H., Lyle, M., Nishi, H., Raffi, I., Gamage, K., Klaus, A., and the Expedition 320/321 Scientists
Proceedings of the Integrated Ocean Drilling Program, Volume 320/321

Data report: a revised biomagnetostratigraphic age model for Site U1338, IODP Expedition 320/321[1]

Jan Backman,[2] Jack G. Baldauf,[3] Marina Ciummelli,[4] and Isabella Raffi[5]

Chapter contents

Abstract

The development of late middle Miocene through recent sedimentation rates was determined for Integrated Ocean Drilling Program Site U1338 in the eastern equatorial Pacific using available geomagnetic chron boundaries and biostratigraphic biohorizons provided by calcareous nannofossils and diatoms. These data were set in a revised depth splice of the three holes at Site U1338 and provide a lower resolution image of the sedimentation rate history in the region of Site U1338 through relatively long linear interpolations between 11 chosen age-depth control points encompassing 18 My. The resulting sedimentation rates depict the movement of Site U1338 from just south of the Equator with modest sedimentation rates starting at 11 m/My to tripling of these rates near 13 Ma, when the site moved onto the Equator and into the equatorial high-productivity belt. High sedimentation rates continued into the earliest Pliocene (5 Ma) except for a 50% decrease during the so-called "carbonate crash" centered around 9.6 Ma ± 0.4 My. The site's movement north, away from the equatorial high-productivity belt, began between 5.0 and 4.2 Ma, when the site was located ~75–90 nmi north of the Equator, and resulted in a series of successively decreasing sedimentation rates to the present rate of 11 m/My, identical to the rate when sedimentation began at Site U1338 at nearly 18 Ma, when the site was located ~100 nmi south of the Equator.

Introduction

A key goal of Integrated Ocean Drilling Program (IODP) Expedition 320/321 (Pacific Equatorial Age Transect [PEAT]) was to recover a series of sediment sections from the Pacific paleoequator region preserving critical intervals of Cenozoic paleoceanographic and paleoclimatic conditions and development (see the **"Expedition 320/321 summary"** chapter [Pälike et al., 2010]). The age transect, or flow-line concept, of Pälike et al. (2010) made use of Pacific plate motion and placed sites close to the Pacific paleoequator for carefully selected time intervals that would ensure near-continuous recovery of optimally preserved early Eocene through recent sediment sections. Eight sites were drilled (Sites U1331–U1338) with present locations along an oblique north–south transect from 12°4′N, 142°10′W (old end-member Site U1331; 5116 m water depth), to 2°30′N, 117°58′W (young end-

[1]Backman, J., Baldauf, J.G., Ciummelli, M., and Raffi, I., 2016. Data report: a revised biomagnetostratigraphic age model for Site U1338, IODP Expedition 320/321. *In* Pälike, H., Lyle, M., Nishi, H., Raffi, I., Gamage, K., Klaus, A., and the Expedition 320/321 Scientists, *Proceedings of the Integrated Ocean Drilling Program,* 320/321: Tokyo (Integrated Ocean Drilling Program Management International, Inc.). doi:10.2204/iodp.proc.320321.219.2016
[2]Department of Geological Sciences, Stockholm University, SE-10691 Stockholm, Sweden. backman@geo.su.se
[3]Department of Oceanography, Texas A&M University, College Station TX 77843, USA.
[4]Petrostrat Ltd., Tan-Y-Graig, Parc Caer Seion, LL32 8FA Conwy, United Kingdom.
[5]Dipartimento di Ingegneria e Geologia, Università "G. d'Annunzio" di Chieti-Pescara, I-66013 Chieti Scalo, Italy.

member Site U1338; 4200 m water depth). Establishing an age model for each site was a crucial component of the expedition objectives.

Sediment sections recovered from three holes at Site U1338 represent the interval from the late early Miocene at ~18 Ma to the recent. These three holes were spliced onboard using physical property data into a single continuous section with coherent depth progression from the water/sediment interface to the sediment–basalt transition, permitting determination of linear sedimentation rates from biomagnetostratigraphic data (see Fig. **F14** in the "Site U1338" chapter [Expedition 320/321 Scientists, 2010b]).

IODP employs three different core depth concepts for recovered sediments. The baseline depth is in meters below seafloor (mbsf), or core depth below seafloor (CSF-A, in meters). When splicing a single continuous section from multiple holes at a single drill site, a second set of depths are assigned to the cores: composite depth below seafloor (CCSF-A, in meters). Empirically, we have learned that CCSF-A depths lie deeper than CSF-A depths and that the spliced section typically has grown in length by about 10%. In the case of Site U1338, this value was 11%, calculated by linear regression of CSF-A versus CCSF-A for all Site U1338 cores (see Fig. **F44** in the "Site U1338" chapter [Expedition 320/321 Scientists, 2010b]). This growth factor distorts sedimentation and mass accumulation rates. To compensate for this distortion, CCSF-A depths for Site U1338 were divided by a growth factor of 1.11, resulting in a third set of depths, the corrected composite depths (CCSF-B, in meters) (see Table **T23** in the "Site U1338" chapter [Expedition 320/321 Scientists, 2010b]). Subsequently, CCSF-A depth data from Site U1338 were revised by **Wilkens et al.** (2013), who also provide a discussion of IODP depth scale terminology.

Here, we combine revised diatom and partly revised calcareous nannofossil biostratigraphic data with shipboard magnetostratigraphic data to produce a biomagnetostratigraphic age model for Site U1338 using the **Wilkens et al.** (2013) revised depth data.

Methods

Shipboard calcareous nannofossil biostratigraphic and magnetostratigraphic data were acquired from all three holes at Site U1338 (see Tables **T4** and **T15** in the "Site U1338" chapter [Expedition 320/321 Scientists, 2010b]). Ciummelli (2013) provided additional higher resolution calcareous nannofossil biostratigraphic data for the late middle through earliest Pliocene interval that were partly published by Backman et al. (2013). **Baldauf** (2013) provided higher resolution diatom biostratigraphic data. See above references for methods of data acquisition. Age estimates and nomenclatures for geomagnetic chron boundaries follow the timescale of Lourens et al. (2004). Age estimates for equatorial Pacific diatom biohorizons were synthesized by Barron (1992) and are here converted from the timescale by Berggren et al. (1985) to that by Lourens et al. (2004). Age estimates for calcareous nannofossils mainly represent astronomically tuned calibrations from the western equatorial Atlantic (Backman et al., 2012).

Results and discussion

Revised CCSF-A depths for both biostratigraphic and magnetostratigraphic data were calculated by adding an offset depth to the CSF-A depth for each core, according to Table **T5** in Wilkens et al. (2013). They further refined depths within cores from all three holes at Site U1338 caused by intracore stretching or squeezing and referred to these depths as "Adjusted CCSF." In Tables **AT47, AT52,** and **AT57,** Wilkens et al. (2013) adjusted depths for a total of 843 samples. Of these samples, 232 show no adjustment (0 cm), 281 show an average adjustment of +16 cm, and 330 show an average adjustment of –17 cm. These adjusted depths within cores are generally small but are useful for exceptionally detailed work in need of centimeter precision. Considering the uncertainties involved in the underlying data sets, we did not employ the "Adjusted CCSF" by **Wilkens et al.** (2013).

Growth factors for each hole are calculated by linear regression (Fig. **F1**) of CSF-A versus CCSF-A, following the approach from the **"Site U1338"** chapter (Expedition 320/321 Scientists, 2010b). The CCSF-A depth is divided by the hole-specific growth factor to obtain the corrected composite CCSF-B depth for each biomagnetostratigraphic age-depth indicator from each hole.

Site U1338 biomagnetostratigraphic age-depth data are presented in Tables **T1** (calcareous nannofossils), **T2** (diatoms), and **T3** (magnetostratigraphy). Many individual biohorizons and magnetostratigraphic chron boundaries have been determined from two or all three Site U1338 holes (see the **"Site U1338"** chapter [Expedition 320/321 Scientists, 2010b]; **Baldauf,** 2013; Ciummelli, 2013; Backman et al., 2013). It is difficult to determine which hole provides the true or most accurate depth information for individual age-depth indicators. Hence, the midpoint of the deepest and shallowest CCSF-B depths are used for individual chron boundaries and biohorizons in the sedimentation rate plots, taking into account one, two, or all three holes from Site U1338. These midpoint CCSF-B depths show average uncertainties of ±1.23 m (maximum ±3.54 m) for calcareous nannofossils, ±0.86 m (maximum ±8.23 m) for diatoms, and ±0.57 m (maximum ±2.32 m) for magnetostratigraphic chron boundaries.

The entire age-depth data set is presented in Figure F2. These data are composed of 33 geomagnetic chron boundaries, 33 calcareous nannofossil biohorizons, and 57 diatom biohorizons. Magnetostratigraphy is available in three different yet coherent intervals: Pliocene–Pleistocene (3.596–0.781 Ma), early late Miocene (9.987–9.098 Ma), and late middle Miocene (15.160–12.730 Ma).

Age calibrations of diatom biohorizons represent lower resolution equatorial Pacific data generated 23 years ago, which may suggest potential room for improvement (as always in biochronology). Still, the diatom biohorizons generally align well with magnetostratigraphic chron boundaries and calcareous nannofossil biohorizons, presumably because 75% of the diatom biohorizons (Table T2) have been directly calibrated with geomagnetic polarity stratigraphies from the equatorial Pacific (Barron, 1992) in depositional settings similar to that of Site U1338. In the 9.0 through 12.9 Ma interval, however, only 23% (3 of 13) of the diatom biohorizons are directly calibrated with magnetostratigraphy.

In order to show details of the different parts of the sedimentation rate history at Site U1338, the record is divided into three parts: 0–5.2 Ma (Fig. F3), 5–10.2 Ma (Fig. F4), and 9.9–18 Ma (Fig. F5). The proposed rate-determining age-depth indicators, or control points (CPs), and the resulting linear sedimentation rates (LSRs) are presented in Table T4.

It appears clearly from Figure F2 that the 123 age-depth indicators fall into coherent linear intervals, albeit with some minor scatter. Minor variations in sedimentation rates presumably occurred in the presented linear intervals between the nearest chosen age-depth CP couplets. It is beyond the scope of this data report to accommodate for such minor variations, which would require highly resolved cyclostratigraphic or stable isotopic data correlated to sites with independent (magnetostratigraphic) age control to resolve properly. When allowing for minor scatter in these biomagnetostratigraphic data, the suggested LSRs become uniform over relatively long intervals. This is considered preferable in comparison to, for example, placing CPs at each progressively deeper age-depth indicator, which would still result in scatter but also cause artificial extremes in sedimentation rates between closely spaced age-depth indicator couplets.

Age estimates of late early Miocene through Pleistocene geomagnetic chron boundaries are considered well constrained (Lourens et al., 2004), yet we have permitted a few such boundaries in the older/deeper part of the record to fall slightly off the proposed interpolated rate lines (Fig. F5) so as to not introduce extreme, shorter variations in sedimentation rates caused by less well constrained depths or age estimates of a few chron boundaries.

With these caveats, this data report may be taken to provide a basic biomagnetostratigraphic reference framework for future attempts to develop highly resolved age models for Site U1338 based on, for example, carbon isotope stratigraphy or astronomically tuned cyclostratigraphy.

We are fully aware of that the relatively few (11) interpolated linear sedimentation rate intervals encompassing the past 18 My at Site U1338 may be drawn differently, yet we consider that the proposed sedimentation rate history represents a reasonable interpretation of the age-depth distribution of available magnetostratigraphic, diatom, and calcareous nannofossil data. All depths below are on the CCSF-B scale.

Sedimentation rate lines between 0 and 5 Ma

Pliocene–Pleistocene sedimentation rates are shown in Figure F3. The youngest rate line is determined by the top of the Site U1338 sediment sequence, placed at 0.00 m and 0.00 Ma, and the Chron C1n/C1r boundary (base Brunhes; CP1).

CP2 is the Chron C2n/C2r.1r boundary (base Olduvai), and CP3 is the Chron C2An.3n/C2Ar boundary (base Gauss). There are two diatom and three calcareous nannofossil biohorizons clearly falling to the left of the proposed rate line between CP2 and CP3, suggesting that these represent paleoecologically driven disappearances prior to their genuine extinctions.

The three nannofossil extinctions represent *Discoaster* species, two of which have known problematic abundance histories toward the end of their ranges in the equatorial Pacific (Backman and Shackleton, 1983). It remains uncertain why the diatom biohorizons at 4.7 Ma (top *Fragilariopsis cylindrica*) and 4.9 Ma (base *Nitzschia jouseae*) deviate from the proposed interpolated line controlled by CP4 (base *Asteromphalus elegans* at 4.2 Ma) and CP5 (top *Ceratolithus acutus* at 5.04 Ma).

Sedimentation rate lines between 5 and 10 Ma

A constant sedimentation rate is suggested over 4 My from CP5 in the earliest Pliocene to CP6 (base Chron CAn) in the early late Miocene (Fig. F4). Two nannofossil biohorizons are clearly off the line, one being the top of the absence interval (paracme) of *Reticulofenestra pseudoumbilicus* (7.09 Ma) and the other the base of *Amaurolithus* spp. (7.39 Ma). Both biohorizons appear unproblematic in terms of abundance patterns (Backman et al., 2013). The former biohorizon does not represent the evolutionary first appearance of the species but rather its reappearance after having been virtually absent from the assemblages for about 1.7 My for reasons unknown. Its position suggests a reduced absence interval of about 0.4 My at its upper end in the region of Site U1338, as the proposed interpolated line suggests a reappearance at 7.5 Ma rather than 7.1 Ma. Base *Amaurolithus* spp. seems to appear at ~0.3 My earlier (7.7 Ma rather than 7.4 Ma) to the Site U1338 region compared with its calibrated first appearance from both the western equatorial Atlantic and two sites in the eastern equatorial Pacific (Backman et al., 2012). In Monte dei Corvi section on the Adriatic Sea coast, base *Amaurolithus* spp. occurs in the middle part of Chron C4n.1n at an estimated age of 7.57 Ma (Di Stefano et al., 2010), which would bring this biohorizon to within 0.1 My from the proposed interpolated line. These data suggest that this biohorizon is diachronous, perhaps up to 0.3 My, as suggested at Site U1338.

The interval between CP6 and CP7 is controlled by geomagnetic chron boundaries, one of which only marginally fits the proposed rate line. Top *Catinaster coalitus* at 9.70 Ma disappeared from the Site U1338 region well prior to its calibrated extinction. Not surprisingly, the final part of its range is characterized by low and discontinuous abundances (Backman et al., 2013).

Sedimentation rate lines between 10 and 18 Ma

The interval between geomagnetic chron boundaries CP7 and CP8 encompasses 3.2 My (Fig. F5). Even if this interval is divided using one or two intermediate biostratigraphic CPs, biohorizons will still be scattered around the shorter interpolation alternative.

Between CP8 and CP9, four geomagnetic chron boundaries do not fit the proposed linear interpolation. Less good core conditions began to affect the splice and composite section toward the deep end of the sequence (see **"Site U1338"** in the "Expedition 320/321 summary" chapter [Pälike et al., 2010]), which presumably affected the positions of some of the deepest geomagnetic chron boundaries. For example, in Holes U1338B and U1338C (Table T3), the series of successively older geomagnetic chron boundaries shows a corresponding successive increase in depth. When combining the data from the two holes to calculate midpoint depths of individual chron boundaries from their lowermost and uppermost occurrences, the obvious progression of depth in the individual holes dissolves, suggesting that the two holes are not perfectly correlated in their deepest parts. The position of, for example, the C5ADr/C5Bn.1n boundary in Hole U1338B at 14.781 Ma occurs above (354.00 m) the younger (14.581 Ma) C5ADn/C5ADr boundary at 356.44 m in Hole U1338C (Table T3). We therefore used only data from Hole U1338C for the four deepest geomagnetic chron boundaries in order to maintain a logical depth progression of each successive chron boundary.

The lowermost part of the Site U1338 sedimentation rate history is based on nannofossil biostratigraphy. The short overlap between two nannofossil biohorizons at 15.69 Ma (*Discoaster deflandrei* decreases to <30% of the total *Discoaster* assemblage) and 15.73 Ma (base *Discoaster signus*) indicates that CP10 can be confidently placed at the latter biohorizon. The base of common *Sphenolithus heteromorphus* provides CP11, which has a consistent first common occurrence in Chron C5Dr in the Indian Ocean, Atlantic Ocean, and Mediterranean Sea (Backman et al., 1990, 2012; Di Stefano et al., 2015).

Sedimentation rates versus age

The sedimentation rate history at Site U1338 shows distinct variability and some general trends (Fig. F6; Table T4). When plotting the sedimentation rate history using linear interpolation between specific age-depth indicators, rates change stepwise at the CPs. We assume that the rate history was more smooth than depicted in Figure F6 and that the changes did not generally occur at the CPs but more likely as transitions between the CPs.

Rates were modest (11 m/My) during the first 2 My of sedimentation at Site U1338, when the site was located ~100 nmi south of the Equator (see Fig. F5 in the "Expedition 320/321 summary" chapter [Pälike et al., 2010]). Sedimentation rates thereafter increased to 34 m/My by ~13.2 Ma, when the site began to approach the Equator from the south. This high rate was maintained for about 3 My until the rate was halved to 17 m/My between 10.0 and 9.1 Ma.

This major yet temporary decrease in sedimentation rate coincides with intense carbonate dissolution at Site U1338, also known as the "carbonate crash," in the eastern equatorial Pacific (Farrell et al., 1995; Lyle et al., 1995). The most intense dissolution occurs over a 0.72 m thick interval within Section 321-U1338B-22H-2, with a minimum carbonate content of 5% and an average of 12% between 198.85 and 199.57 m (**Lyle and Backman,** 2013) corresponding to a 42 ky long interval according to the present age model, beginning at 9.618 Ma and ending at 9.576 Ma.

Carbonate content and the sedimentation rate increased after this early late Miocene carbonate crash at ~9.6 Ma to 30 m/My for a 4.1 My long interval lasting into the earliest Pliocene. This late Miocene rate regime changed in the early Pliocene between 5.0 and 4.2 Ma into a new Pliocene–Pleistocene sedimentation rate regime with an average of 14 m/My representing a decrease of 56% compared with the late Miocene regime. Exactly when this major decrease occurs is unclear. If extrapolating the late Miocene regime upward and the early Pliocene regime downward, these will meet at ~4.8 Ma, when the site was located ~80 nmi north of the Equator (see Fig. **F5** in the "Expedition 320/321 summary" chapter [Pälike et al., 2010]).

Pliocene–Pleistocene sedimentation rates are, however, not uniform, but they show a stepwise decrease from 18 m/My (5.0–4.2 Ma) to 15 m/My (4.2–3.6 Ma), followed by 13 m/My (3.6–1.9 Ma) to 12 m/My (1.9–0.8 Ma) and finally 11 m/My (0.8–0.0 Ma), as Site U1338 is slowly moving away from the Equatorial high productivity region.

Conclusions

Late middle Miocene through recent linear sedimentation rates were calculated for IODP Site U1338 in the eastern equatorial Pacific using available geomagnetic chron boundary data together with calcareous nannofossil and diatom biochronologic data. Rather than attempting to use every age-depth indicator for estimates of sedimentation rates, we selected 11 key control points to describe a low-resolution sedimentation history, thus permitting for scatter around the proposed interpolated rate lines.

The sedimentation rate history at Site U1338 mirrors the movement of the site from ~2°45′S of the Pacific Equator to its present location at 2°30′N of the Equator, crossing a high-productivity zone during the late middle Miocene through earliest Pliocene times and resulting in sedimentation rates on the order of 30–34 m/My. Sedimentation rates started at a modest rate (11 m/My) when the Site U1338 basalt crust was formed, ramped up in three steps to a tripling at ~13.2 Ma to 34 m/My, and decreased by 50% during the so-called carbonate crash between 10.0 and 9.1 Ma. The crash was followed by an increase to 30 m/My that lasted for ~4 My into the earliest Pliocene (5.0 Ma). Thereafter, sedimentation rates decreased successively in five steps to its present rate of 11 m/My.

Acknowledgments

This research used data and samples provided by the Integrated Ocean Drilling Program (IODP). J. Backman acknowledges financial support from the Swedish Research Council and Stockholm University. Reviews by Samantha Gibbs and Anna Joy Drury helped improve the manuscript.

References

Backman, J., Raffi, I., Ciummelli, M., and Baldauf, J., 2013. Species-specific responses of late Miocene *Discoaster* spp. to enhanced biosilica productivity conditions in the equatorial Pacific and the Mediterranean. *Geo-Marine Letters,* 33(4):285–298. **http://dx.doi.org/10.1007/s00367-013-0328-0**

Backman, J., Raffi, I., Rio, D., Fornaciari, E., and Pälike, H., 2012. Biozonation and biochronology of Miocene through Pleistocene calcareous nannofossils from low and middle latitudes. *Newsletters on Stratigraphy,* 45(3):221–244. **http://dx.doi.org/10.1127/0078-0421/2012/0022**

Backman, J., Schneider, D.A., Rio, D., and Okada, H., 1990. Neogene low-latitude magnetostratigraphy from Site 710 and revised age estimates of Miocene nannofossil datum events. *In* Duncan, R.A., Backman, J., Peterson, L.C., et al., *Proceedings of the Ocean Drilling Program, Scientific Results,* 115: College Station, TX (Ocean Drilling Program), 271–276. **http://dx.doi.org/10.2973/odp.proc.sr.115.209.1990**

Backman, J., and Shackleton, N.J., 1983. Quantitative biochronology of Pliocene and early Pleistocene calcareous nannofossils from the Atlantic, Indian and Pacific Oceans. *Marine Micropaleontology,* 8(2):141–170. **http://dx.doi.org/10.1016/0377-8398(83)90009-9**

Baldauf, J.G., 2013. Data report: diatoms from Sites U1334 and U1338, Expedition 320/321. *In* Pälike, H., Lyle, M., Nishi, H., Raffi, I., Gamage, K., Klaus, A., and the Expedition 320/321 Scientists, *Proceedings of the Integrated Ocean Drilling Program,* 320/321: Tokyo (Integrated Ocean Drilling Program Management International, Inc.). **http://dx.doi.org/10.2204/iodp.proc.320321.215.2013**

Barron, J.A., 1992. Neogene diatom datum levels in the equatorial and North Pacific. *In* Ishizaki, K., and Saito, T. (Eds.), *Centenary of Japanese Micropaleontology:* Tokyo (Terra Scientific Publishing Company), 413–425. **http://www.terrapub.co.jp/e-library/cjm/pdf/0413.pdf**

Berggren, W.A., Kent, D.V., and Van Couvering, J.A., 1985. The Neogene, Part 2. Neogene geochronology and chronostratigraphy. *In* Snelling, N.J. (Ed.), *The Chronology of the Geological Record.* Memoir—Geological Society of London, 10:211–260. **http://dx.doi.org/10.1144/GSL.MEM.1985.010.01.18**

Ciummelli, M., 2013. Morphometry, evolution, biostratigraphy and paleoecology of the genus *Discoaster* in the Miocene using material from Site U1338, IODP Exp. 321 [Ph.D. dissertation]. University of Chieti-Pescara, Italy.

Di Stefano, A., Baldassini, N., Maniscalco, R., Speranza, F., Maffione, M., Cascella, A., and Foresi, L.M., 2015. New bio-magnetostratigraphic data on the Miocene Moria section (Northern Apennines, Italy): connections between the Mediterranean region and the North Atlantic Ocean. *Newsletters on Stratigraphy*, 48(2):135–152. **http://dx.doi.org/10.1127/nos/2015/0057**

Di Stefano, A., Verducci, M., Lirer, F., Ferraro, L., Iaccarino, S.M., Hüsing, S.K., and Hilgen, F.J., 2010. Paleoenvironmental conditions preceding the Messinian Salinity Crisis in the central Mediterranean: integrated data from the upper Miocene Trave section (Italy). *Palaeogeography, Palaeoclimatology, Palaeoecology*, 297(1):37–53. **http://dx.doi.org/10.1016/j.palaeo.2010.07.012**

Expedition 320/321 Scientists, 2010a. Methods. *In* Pälike, H., Lyle, M., Nishi, H., Raffi, I., Gamage, K., Klaus, A., and the Expedition 320/321 Scientists, *Proceedings of the Integrated Ocean Drilling Program,* 320/321: Tokyo (Integrated Ocean Drilling Program Management International, Inc.). **http://dx.doi.org/10.2204/iodp.proc.320321.102.2010**

Expedition 320/321 Scientists, 2010b. Site U1338. *In* Pälike, H., Lyle, M., Nishi, H., Raffi, I., Gamage, K., Klaus, A., and the Expedition 320/321 Scientists, *Proceedings of the Integrated Ocean Drilling Program,* 320/321: Tokyo (Integrated Ocean Drilling Program Management International, Inc.). **http://dx.doi.org/10.2204/iodp.proc.320321.110.2010**

Farrell, J.W., Raffi, I., Janecek, T.R., Murray, D.W., Levitan, M., Dadey, K.A., Emeis, K.-C., Lyle, M., Flores, J.-A., and Hovan, S., 1995. Late Neogene sedimentation patterns in the eastern equatorial Pacific Ocean. *In* Pisias, N.G., Mayer, L.A., Janecek, T.R., Palmer-Julson, A., and van Andel, T.H. (Eds.), *Proceedings of the Ocean Drilling Program, Scientific Results,* 138: College Station, TX (Ocean Drilling Program), 717–756. **http://dx.doi.org/10.2973/odp.proc.sr.138.143.1995**

Lourens, L.J., Hilgen, F.J., Shackleton, N.J., Laskar, J., and Wilson, D., 2004. The Neogene period. *In* Gradstein, F.M., Ogg, J.G., and Smith, A.G. (Eds.), *A Geological Time Scale 2004*. Cambridge, UK (Cambridge Univ. Press), 409–440.

Lyle, M., and Backman, J., 2013. Data report: calibration of XRF-estimated $CaCO_3$ along the Site U1338 splice. *In* Pälike, H., Lyle, M., Nishi, H., Raffi, I., Gamage, K., Klaus, A., and the Expedition 320/321 Scientists, *Proceedings of the Integrated Ocean Drilling Program,* 320/321: Tokyo (Integrated Ocean Drilling Program Management International, Inc.). **http://dx.doi.org/10.2204/iodp.proc.320321.205.2013**

Lyle, M., Dadey, K.A., and Farrell, J.W., 1995. The late Miocene (11–8 Ma) eastern Pacific carbonate crash: evidence for reorganization of deep-water circulation by the closure of the Panama gateway. *In* Pisias, N.G., Mayer, L.A., Janecek, T.R., Palmer-Julson, A., and van Andel, T.H. (Eds.), *Proceedings of the Ocean Drilling Program, Scientific Results,* 138: College Station, TX (Ocean Drilling Program), 821–838. **http://dx.doi.org/10.2973/odp.proc.sr.138.157.1995**

Pälike, H., Nishi, H., Lyle, M., Raffi, I., Gamage, K., Klaus, A., and the Expedition 320/321 Scientists, 2010. Expedition 320/321 summary. *In* Pälike, H., Lyle, M., Nishi, H., Raffi, I., Gamage, K., Klaus, A., and the Expedition 320/321 Scientists, *Proceedings of the Integrated Ocean Drilling Program,* 320/321: Tokyo (Integrated Ocean Drilling Program Management International, Inc.). **http://dx.doi.org/10.2204/iodp.proc.320321.101.2010**

Raffi, I., Backman, J., Fornaciari, E., Pälike, H., Rio, D., Lourens, L., and Hilgen, F., 2006. A review of calcareous nannofossil astrobiochronology encompassing the past 25 million years. *Quaternary Science Reviews,* 25(23–24):3113–3137. **http://dx.doi.org/10.1016/j.quascirev.2006.07.007**

Wilkens, R.H., Dickens, G.R., Tian, J., Backman, J., and the Expedition 320/321 Scientists, 2013. Data report: revised composite depth scales for Sites U1336, U1337, and U1338. *In* Pälike, H., Lyle, M., Nishi, H., Raffi, I., Gamage, K., Klaus, A., and the Expedition 320/321 Scientists, *Proceedings of the Integrated Ocean Drilling Program,* 320/321: Tokyo (Integrated Ocean Drilling Program Management International, Inc.). **http://dx.doi.org/10.2204/iodp.proc.320321.209.2013**

Initial receipt: 8 September 2015
Acceptance: 5 November 2015
Publication: 11 February 2016
MS 320321-219

Figure F1. CSF-A versus CCSF-A depths for tops of cores, Site U1338. Growth factors = slope of the regression line for each hole.

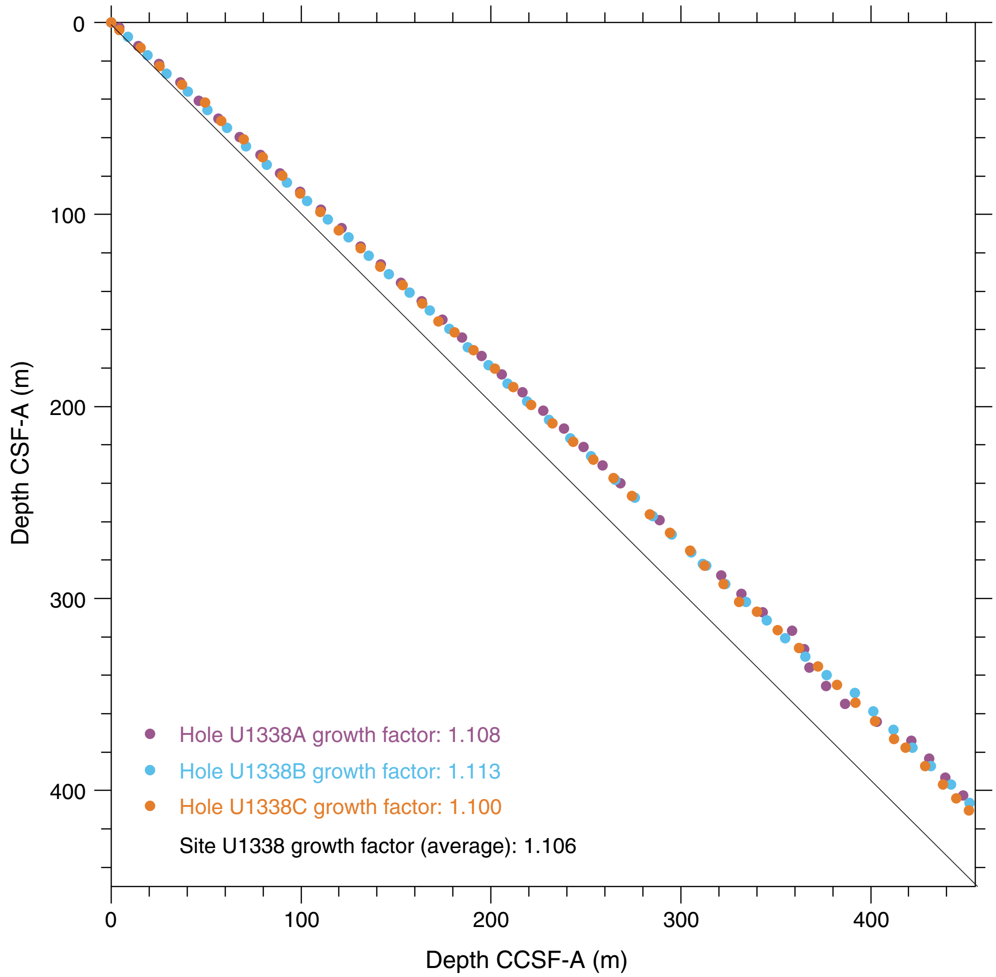

Figure F2. Biomagnetostratigraphic indicators, 0–18 Ma, Site U1338. Symbols are shown with error bars in the depth domain, representing the lowermost and uppermost depths of biohorizons and chron boundaries (Tables T1, T2, T3).

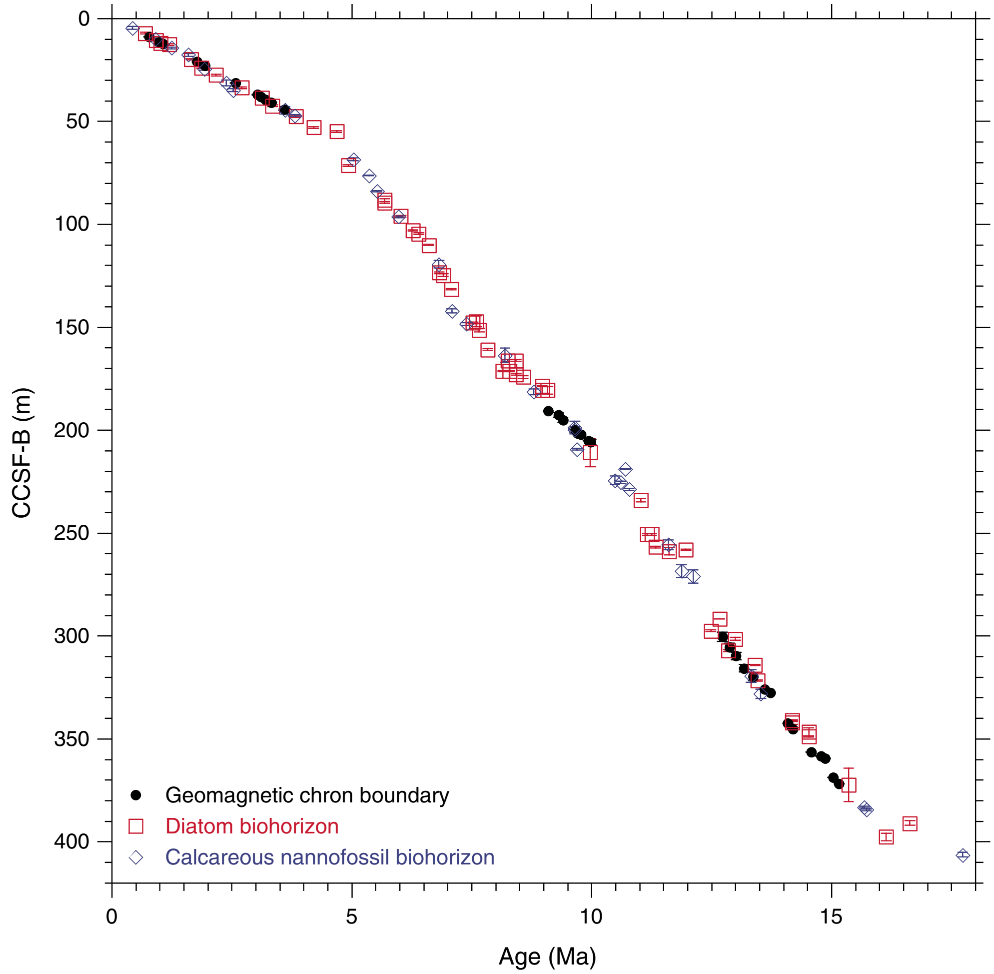

Figure F3. Biomagnetostratigraphic indicators, 0–5.2 Ma, Site U1338. See Table **T4** for CPs and LSRs. Symbols are shown with error bars in the depth domain, representing the lowermost and uppermost depths of biohorizons and chron boundaries (Tables **T1, T2, T3**).

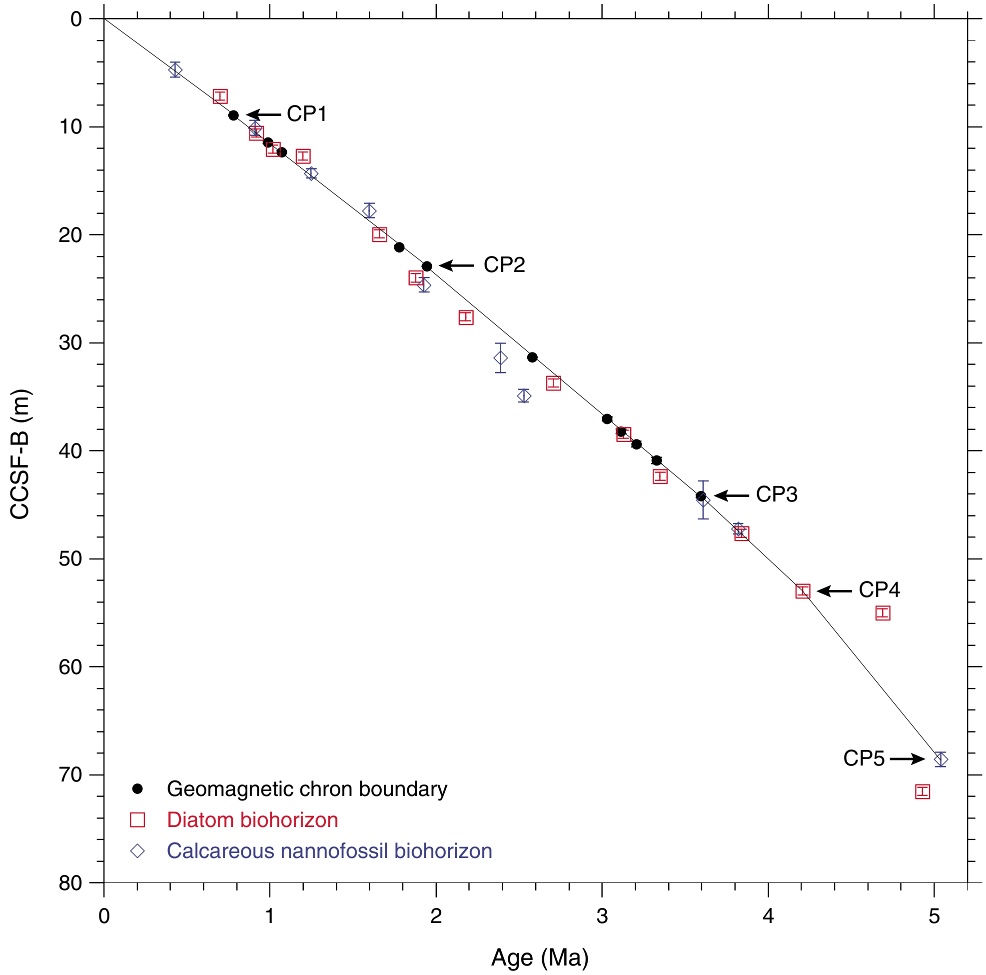

Figure F4. Biomagnetostratigraphic indicators, 5.0–10.2 Ma, Site U1338. See Table T4 for CPs and LSRs. Symbols are shown with error bars in the depth domain, representing the lowermost and uppermost depths of biohorizons and chron boundaries (Tables T1, T2, T3).

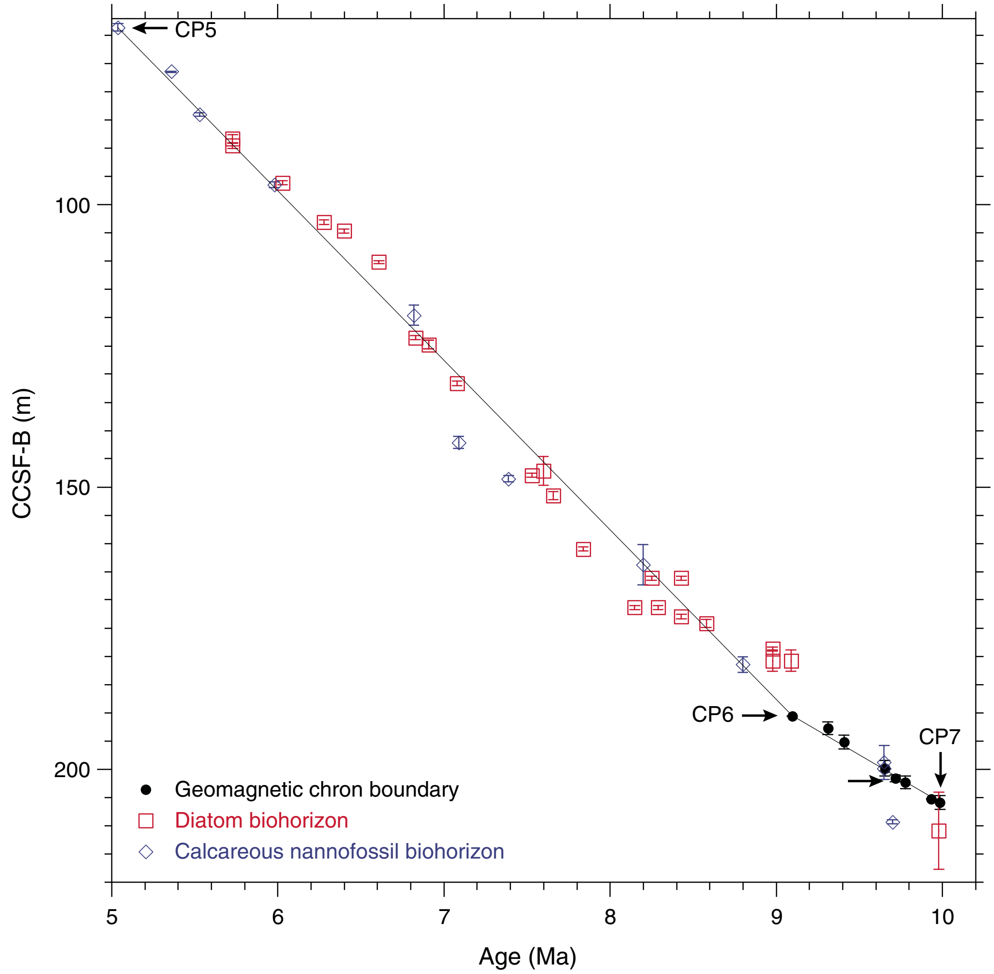

Figure F5. Biomagnetostratigraphic indicators, 10–18 Ma, Site U1338. See Table T4 for CPs and LSRs. Site U1338 terminal depth = 413.6 m CCSF-B at 18.4 Ma. Symbols are shown with error bars in the depth domain, representing the lowermost and uppermost depths of biohorizons and chron boundaries (Tables T1, T2, T3).

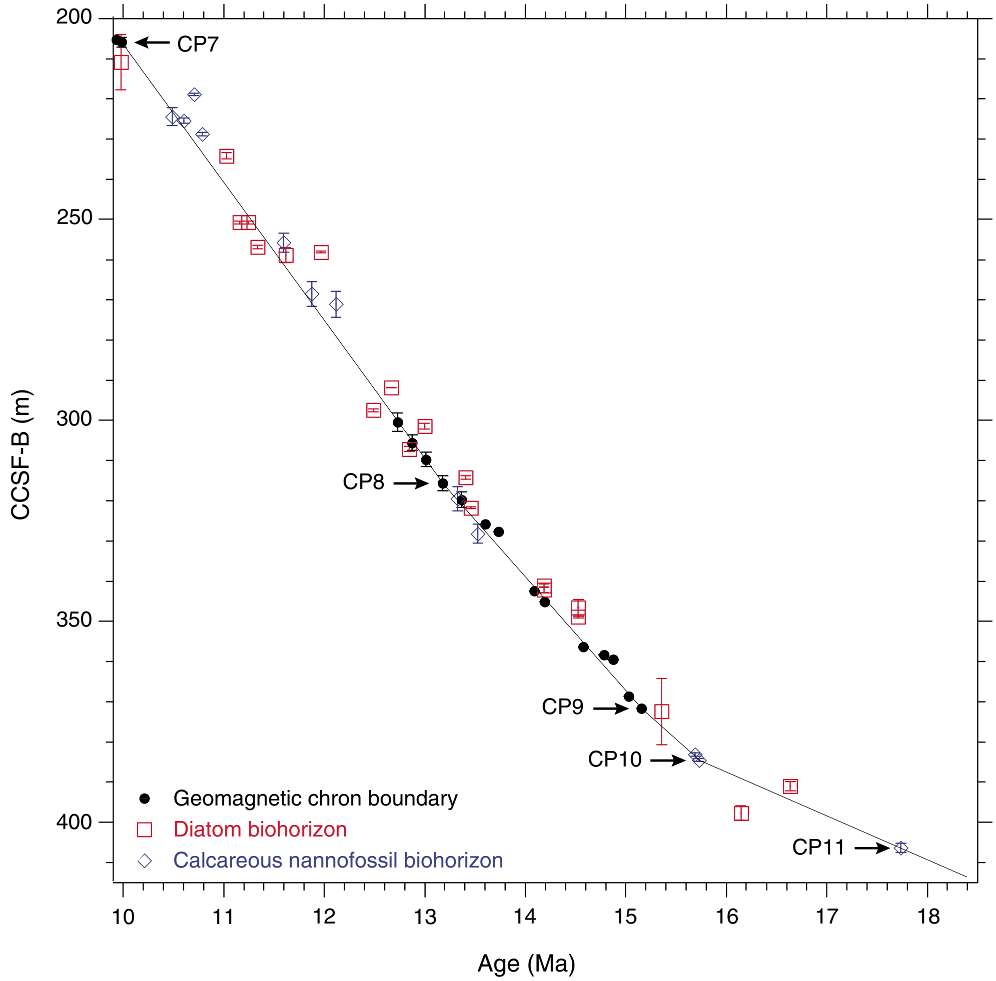

Figure F6. Linear sedimentation rate versus age. CP numbers in plot refer to Table T4. Estimated paleolatitude positions of Site U1338 are from Figure F5 in the "Expedition 320/321 summary" chapter (Pälike et al., 2010).

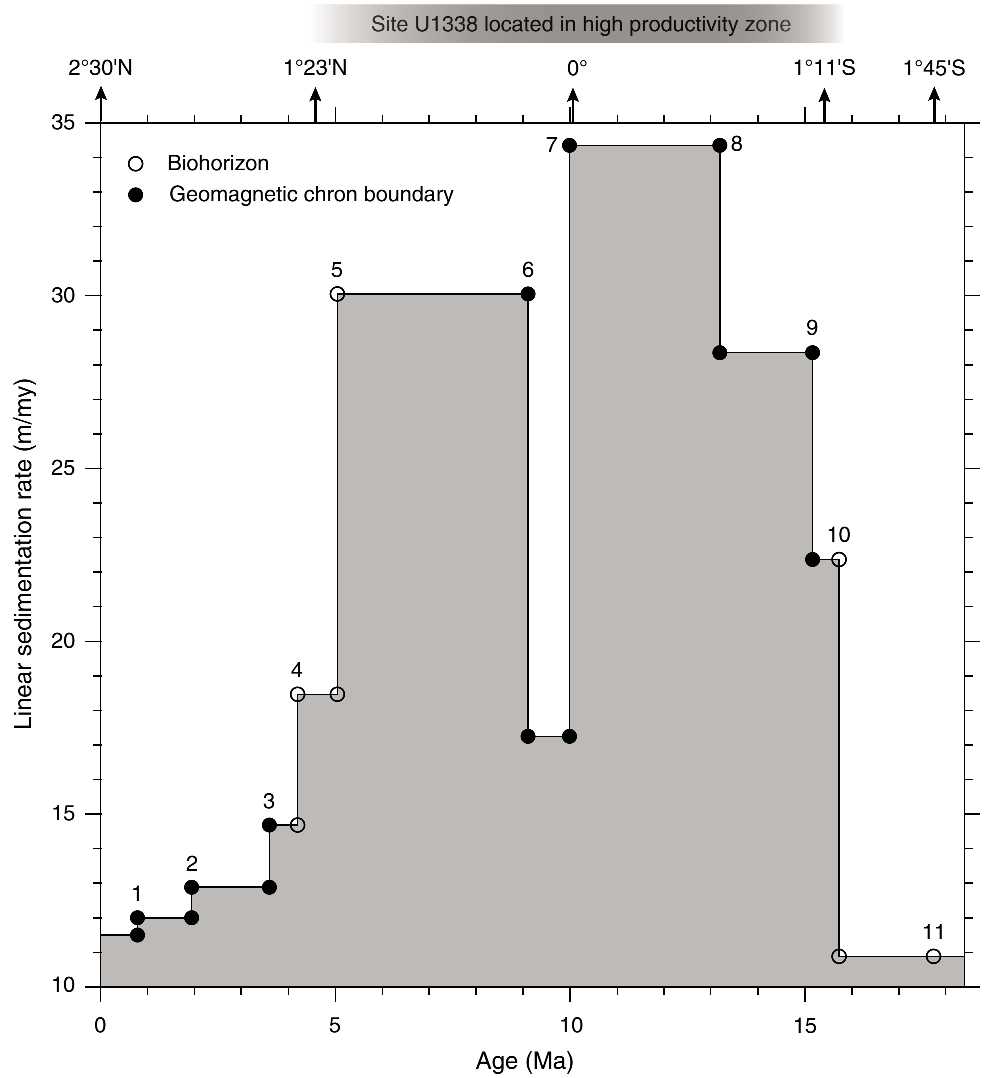

Table T1. Biomagnetostratigraphic age-depth data for calcareous nannofossils, Site U1338. This table is available in **oversized format.**

Table T2. Biomagnetostratigraphic age-depth data for diatoms, Site U1338.

Diatom biohorizon	Age (Ma)	Top hole, core, section, interval (cm)	Bottom hole, core, section, interval (cm)	Top depth CSF-A (m)	Bottom depth CSF-A (m)	Top depth CCSF-A (m)	Bottom depth CCSF-A (m)	Revised depth (midpoint) CCSF-B (m)	Uncertainty (± m)	Calibrated with magneto-stratigraphy
		321-	321-							
T *Fragilariopsis reinholdii*	0.70	U1338A-2H-3, 45	U1338A-2H-3, 120	6.15	6.90	7.63	8.38	**7.22**	0.38	Yes
T *Fragilariopsis fossilis*	0.92	U1338A-2H-5, 120	U1338A-2H-6, 45	9.90	10.65	11.38	12.13	**10.61**	0.38	No
T *Rhizosolenia matuyamai*	1.02	U1338B-2H-3, 120	U1338B-2H-4, 45	11.80	12.55	13.09	13.84	**12.10**	0.38	Yes
B *Rhizosolenia matuyamai*	1.2	U1338B-2H-4, 45	U1338B-2H-4, 120	12.55	13.30	13.84	14.59	**12.77**	0.38	Yes
T *Rhizosolenia praebergonii* var. *robusta*	1.66	U1338B-3H-2, 120	U1338B-3H-3, 45	19.80	20.55	21.87	22.62	**19.99**	0.38	Yes
B *Fragilariopsis doliolus*	1.9	U1338B-3H-5, 120	U1338B-3H-6, 45	24.30	25.05	26.37	27.12	**24.03**	0.38	Yes
T *Thalassiosira convexa var. convexa*	2.2	U1338A-4H-4, 45	U1338A-4H-4, 120	26.65	27.40	30.27	31.02	**27.66**	0.38	Yes
T *Nitzschia jouseae*	2.7	U1338A-5H-1, 45	U1338A-5H-1, 120	31.65	32.40	37.05	37.80	**33.78**	0.38	Yes
B *Rhizosolenia praebergonii var. robusta*	3.1	U1338A-5H-4, 120	U1338A-5H-5, 45	36.90	37.65	42.30	43.05	**38.52**	0.38	Yes
T *Actinocyclus ellipticus* f. *lanceolata*	3.4	U1338B-5H-5, 45	U1338B-5H-5, 120	42.55	43.30	46.85	47.60	**42.43**	0.38	No
B *Thalassiosira convexa* var. *convexa*	3.8	U1338B-6H-2, 45	U1338B-6H-2, 120	47.55	48.30	52.69	53.44	**47.68**	0.38	Yes
B *Asteromphalus elegans*	4.2	U1338A-7H-2, 45	U1338A-7H-2, 120	52.15	52.90	58.36	59.11	**53.01**	0.38	Yes
T *Fragilariopsis cylindrica*	4.7	U1338A-7H-3, 120	U1338A-7H-4, 45	54.40	55.15	60.61	61.36	**55.04**	0.38	Yes
B *Nitzschia jouseae*	4.9	U1338B-8H-6, 45	U1338A-9H-1, 120	72.55	70.40	79.13	79.85	**71.58**	0.36	Yes
B *Shionodiscus oestrupii*	5.7	U1338B-10H-4, 45	U1338B-10H-5, 45	88.55	90.05	97.55	99.05	**88.32**	0.75	Yes
T *Thalassiosira miocenica*	5.7	U1338B-10H-5, 45	U1338A-11H-1, 45	90.05	88.65	99.05	99.93	**89.59**	0.44	Yes
T *Asterolampra acutiloba*	6.03	U1338B-11H-3, 45	U1338B-11H-3, 120	96.55	97.30	106.67	107.42	**96.18**	0.38	Yes
T *Fragilariopsis miocenica*	6.28	U1338A-12H-3, 45	U1338A-12H-3, 120	101.15	101.90	113.90	114.65	**103.14**	0.38	Yes
T *Nitzschia miocenica* var. *elongata*	6.40	U1338B-12H-2, 45	U1338B-12H-2, 120	104.55	105.30	116.14	116.89	**104.69**	0.38	Yes
T *Thalassiosira praeconvexa*	6.6	U1338B-12H-6, 45	U1338A-13H-1, 120	110.55	108.40	122.14	122.67	**110.23**	0.27	Yes
T *Rossiella praepaleacea*	6.8	U1338C-14H-3, 122	U1338C-14H-4, 47	122.02	122.77	135.60	136.35	**123.61**	0.38	Yes
B *Thalassiosira miocenica*	6.9	U1338B-14H-2, 120	U1338B-14H-3, 120	124.30	125.80	138.20	139.70	**124.84**	0.75	Yes
B *Thalassiosira convexa*	6.9	U1338B-14H-2, 120	U1338B-14H-3, 120	124.30	125.80	138.20	139.70	**124.84**	0.75	Yes
B *Thalassiosira praeconvexa*	7.1	U1338A-15H-3, 45	U1338A-15H-3, 120	129.65	130.40	145.50	146.25	**131.66**	0.38	Yes
T *Nitzschia porteri*	7.5	U1338B-16H-5, 120	U1338B-16H-6, 45	147.80	148.55	164.33	165.08	**147.98**	0.38	Yes
B *Fragilariopsis miocenica*	7.60	U1338A-16H-6, 45	U1338A-17H-2, 45	143.65	147.15	160.56	165.68	**147.22**	2.56	Yes
T *Rossiella paleacea*	7.7	U1338A-17H-3, 45	U1338A-17H-4, 45	148.65	150.15	167.18	168.68	**151.56**	0.75	Yes
T *Thalassiosira burckliana*	7.8	U1338A-18H-3, 45	U1338A-18H-3, 120	158.15	158.90	178.03	178.78	**161.02**	0.38	Yes
B *Fragilariopsis reinholdii*	8.2	U1338B-19H-2, 120	U1338B-19H-3, 45	171.80	172.55	190.40	191.15	**171.41**	0.38	Yes
T *Actinocyclus ellipticus* var. *javanica*	8.25	U1338B-18H-5, 45	U1338B-18H-5, 120	166.05	166.80	184.61	185.36	**166.20**	0.38	Yes
B *Alveus marinus*	8.3	U1338B-19H-2, 120	U1338B-19H-3, 45	171.80	172.55	190.40	191.15	**171.41**	0.38	Yes
T *Thalassiosira yabei*	8.43	U1338B-18H-5, 45	U1338B-18H-5, 120	166.05	166.80	184.61	185.36	**166.20**	0.38	Yes
B *Fragilariopsis cylindrica*	8.43	U1338A-19H-5, 45	U1338A-19H-5, 120	170.65	171.40	191.30	192.05	**172.99**	0.38	Yes
B *Azpeitia nodulifera* var. *cyclopa*	8.6	U1338A-19H-6, 45	U1338B-19H-5, 45	172.15	175.55	192.80	194.15	**174.22**	0.67	Yes
B *Fragilariopsis fossilis*	9.0	U1338A-20H-3, 45	U1338A-20H-5, 120	177.15	180.90	198.44	202.19	**180.79**	1.88	No
B *Thalassiosira yabei* var. *elliptica*	9.0	U1338A-20H-2, 120	U1338A-20H-3, 45	176.40	177.15	197.69	198.44	**178.76**	0.38	No
B *Thalassiosira burckliana*	9.1	U1338A-20H-3, 45	U1338A-20H-5, 120	177.15	180.90	198.44	202.19	**180.79**	1.88	Yes
T *Actinocyclus moronensis*	10.0	U1338B-22H-6, 70	U1338A-24H-2, 108	205.80	214.28	227.42	241.11	**210.95**	6.85	Yes
T *Cavitatus jouseana*	11.0	U1338B-25H-5, 45	U1338A-26H-2, 45	232.55	232.65	259.26	260.93	**234.21**	0.83	No
T *Craspedodiscus coscinodiscus*	11.2	U1338C-28H-1, 122	U1338C-28H-2, 47	248.02	248.77	275.48	276.23	**250.78**	0.38	No
T *Coscinodiscus gigas* var. *diorama*	11.3	U1338C-28H-1, 122	U1338C-28H-2, 47	248.02	248.77	275.48	276.23	**250.78**	0.38	No
T *Actinocyclus ellipticus* var. *spiralis*	11.3	U1338C-28H-6, 47	U1338C-28H-6, 122	254.77	255.52	282.23	282.98	**256.91**	0.38	No
B *Hemidiscus cuneiformis*	11.6	U1338B-28H-1, 120	U1338B-28H-4, 45	258.30	262.05	286.35	290.10	**258.96**	1.88	Yes
T *Actinocyclus ingens*	12.0	U1338C-28H-7, 47	U1338C-29H-1, 47	256.27	256.77	283.73	284.23	**258.16**	0.25	No
T *Crucidenticula nicobarica*	12.5	U1338B-33H-5, 120	U1338B-33H-6, 45	299.60	300.35	330.75	331.50	**297.51**	0.38	No
T *Annellus californicus*	12.7	U1338C-33H-1, 47	U1338B-32H-7, 45	292.87	292.35	322.91	322.97	**291.86**	0.03	No
B *Coscinodiscus gigas* var. *diorama*	12.9	U1338B-34H-4, 45	U1338C-35H-1, 47	306.85	307.37	339.28	340.50	**307.18**	0.61	No
T *Araniscus lewisianus*	13.0	U1338B-34H-1, 45	U1338B-34H-2, 45	302.35	303.85	334.78	336.28	**301.46**	0.75	Yes
T *Thalassiosira tappanae*	13.41	U1338B-35H-3, 120	U1338B-35H-4, 45	315.60	316.35	349.38	350.13	**314.25**	0.38	Yes
B *Azpeitia nodulifera*	13.5	U1338C-36H-4, 47	U1338B-36H-1, 120	321.37	322.10	355.94	356.24	**321.82**	0.15	Yes
T *Cestodiscus peplum*	14.2	U1338C-38H-2, 122	U1338C-38H-3, 47	338.12	338.87	374.91	375.66	**341.17**	0.38	Yes
B *Actinocyclus ellipticus* var. *spiralis*	14.2	U1338C-38H-3, 47	U1338C-38H-4, 47	338.87	340.37	375.66	377.16	**342.19**	0.75	No
B *Thalassiosira tappanae*	14.5	U1338C-39H-1, 122	U1338C-39H-2, 45	346.12	346.85	383.42	384.15	**348.90**	0.36	Yes
T *Coscinodiscus blysmos*	14.5	U1338C-38H-5, 122	U1338C-39H-1, 122	342.62	346.12	379.41	383.42	**346.74**	2.00	No
B *Actinocyclus ingens*	15.4	U1338C-40H-7, 47	U1338C-42H-4, 120	363.87	379.10	401.55	418.01	**372.53**	8.23	No
B *Crucidenticula kanayae*	16.6	U1338C-44H-1, 45	U1338C-44H-2, 120	387.85	390.10	429.06	431.31	**391.08**	1.13	Yes
B *Cestodiscus peplum*	16.2	U1338C-44H-5, 120	U1338C-45H-1, 120	394.60	398.10	435.81	439.31	**397.78**	1.75	Yes

Age column data are from Barron (1992; table 1, including decimal precision) converted to Lourens et al. (2004) timescale. Top and bottom hole, core, section, interval measurements are from Table T3 in Baldauf (2013). Top and bottom CSF-A and CCSF-A depths are from Table T5 in Wilkens et al. (2013). Revised depth = midpoint CCSF-A (m)/site growth factor (Fig. F1). Calibration data are from Barron (1992). Bold = shallowest and deepest depths of individual biohorizons.

Table T3. Biomagnetostratigraphic age-depth data based on magnetostratigraphy, Site U1338.

Geomagnetic polarity chron boundary	Age (Ma)	Core, section, interval (cm)	Depth CSF-A (m)	Depth CCSF-A (m)	Revised depth CCSF-B (m)	Core, section, interval (cm)	Depth CSF-A (m)	Depth CCSF-A (m)	Revised depth CCSF-B (m)	Core, section, interval (cm)	Depth CSF-A (m)	Depth CCSF-A (m)	Revised depth CCSF-B (m)	Top depth Site U1338 CCSF-B (m)	Bottom depth Site U1338 CCSF-B (m)	Depth (midpoint) CCSF-B (m)	Depth uncertainty (± m)
		321-U1338A-				321-U1338B-				321-U1338C-							
C1n/C1r.1r	0.781	2H-4, 122	8.42	9.90	**8.94**	2H-1, 115	8.75	10.04	9.02	2H-4, 105	9.38	9.93	**9.03**	**8.94**	**9.03**	**8.98**	0.05
C1r.1r/C1r.1n	0.988	2H-6, 92	11.12	12.60	**11.37**	2H-3, 85	11.45	12.74	11.45	2H-6, 87	12.17	12.72	**11.56**	**11.37**	**11.56**	**11.47**	0.10
C1r.1n/C1r.2r	1.072	2H-7, 42	12.12	13.60	**12.27**	2H-4, 27	12.37	13.66	12.27	2H-7, 40	13.20	13.75	**12.50**	**12.27**	**12.50**	**12.39**	0.11
C1r.3r/C2n	1.778	3H-7, 0	21.20	23.43	21.15	3H-3, 120	21.30	23.37	**21.00**	3H-6, 40	21.20	23.51	**21.37**	**21.00**	**21.37**	**21.19**	0.19
C2n/C2r.1r	1.945					3H-5, 37	23.47	25.54	22.95	3H-7, 67	22.97	25.28	**22.98**	**22.95**	**22.98**	**22.96**	0.02
C2r.2r/C2An.1n	2.581	4H-7, 48	31.18	34.80	**31.41**	4H-4, 112	32.22	34.88	**31.34**					**31.34**	**31.41**	**31.37**	0.03
C2An.1n/C2An.1r	3.032	5H-3, 130	35.50	40.90	**36.91**	5H-1, 75	36.85	41.15	36.97	5H-3, 47	35.77	41.03	**37.30**	**36.91**	**37.30**	**37.11**	0.19
C2An.1r/C2An.2n	3.116	5H-5, 0	37.20	42.60	**38.45**	5H-2, 40	38.00	42.30	**38.01**	5H-4, 17	36.97	42.23	38.39	**38.01**	**38.45**	**38.23**	0.22
C2An.2n/C2An.2r	3.207					5H-3, 18	39.28	43.58	**39.16**	5H-5, 10	38.40	43.66	**39.69**	**39.16**	**39.69**	**39.42**	0.27
C2An.2r/C2An.3	3.330	5H-6, 140	40.10	45.50	41.06	5H-4, 32	40.92	45.22	**40.63**	5H-6, 30	40.10	45.36	**41.24**	**40.63**	**41.24**	**40.93**	0.30
C2An.3n/C2Ar	3.596	6H-2, 140	43.60	49.16	**44.37**	5H-6, 120	44.80	49.10	**44.12**					**44.12**	**44.37**	**44.24**	0.13
C4An/C4Ar.1r	9.098									21H-6, 15	187.95	209.66	**190.60**	**190.60**	**190.60**	**190.60**	0.00
C4Ar.1r/C4Ar.1n	9.312	21H-6, 10	190.80	213.29	192.50	21H-4, 0	192.60	213.35	**191.69**	22H-1, 140	191.20	213.33	**193.94**	**191.69**	**193.94**	**192.81**	1.12
C4Ar.1n/C4Ar.2r	9.409	22H-1, 10	192.80	216.70	195.58	21H-5, 110	195.20	215.95	**194.03**	22H-3, 112	193.92	216.05	**196.41**	**194.03**	**196.41**	**195.22**	1.19
C4Ar.2r/C4Ar.2n	9.656	22H-3, 122	196.92	220.82	199.30	22H-2, 22	199.32	220.94	**198.51**	22H-7, 50	199.30	221.43	**201.30**	**198.51**	**201.30**	**199.90**	1.40
C4Ar.2n/C4Ar.3r	9.717	22H-5, 10	198.80	222.70	**200.99**	22H-3, 60	201.20	222.82	200.20	23H-1, 125	200.55	222.53	**202.30**	**200.99**	**202.30**	**201.65**	0.65
C4Ar.3r/C5n.1n	9.779					22H-4, 22	202.32	223.94	**201.20**	23H-2, 105	201.85	223.83	**203.48**	**201.20**	**203.48**	**202.34**	1.14
C5n.1n/ C5n.1r	9.934	23H-1, 15	202.35	227.54	**205.36**									**205.36**	**205.36**	**205.36**	0.00
C5n.1r/C5n.2n	9.987					22H-6, 117	206.27	227.89	**204.75**	23H-5, 57	205.87	227.85	**207.14**	**204.75**	**207.14**	**205.94**	1.19
C5Ar.1r/C5Ar.1n	12.730					33H-6, 87	300.77	331.92	**298.22**	34H-2, 95	304.35	333.14	**302.85**	**298.22**	**302.85**	**300.54**	2.32
C5Ar.2n/C5Ar.3r	12.878					34H-3, 67	305.57	338.00	**303.68**	34H-6, 17	309.57	338.36	**307.60**	**303.68**	**307.60**	**305.64**	1.96
C5Ar.3r/C5AAn	13.015					34H-6, 90	310.30	342.73	**307.93**	35H-2, 125	309.65	342.78	**311.62**	**307.93**	**311.62**	**309.78**	1.84
C5AAn/C5AAr	13.183					35H-3, 117	315.57	349.35	**313.88**	35H-7, 35	316.25	349.38	**317.62**	**313.88**	**317.62**	**315.75**	1.87
C5AAr/C5ABn	13.369					35H-6, 110	320.00	353.78	**317.86**	36H-2, 140	319.30	353.87	**321.70**	**317.86**	**321.70**	**319.78**	1.92
C5ABn/C5ABr	13.605					36H-6, 15	328.59	362.73	**325.90**					**325.90**	**325.90**	**325.90**	0.00
C5ABr/C5ACn	13.734					36H-7, 65	330.55	364.69	**327.66**					**327.66**	**327.66**	**327.66**	0.00
C5ACn/C5ACr	14.095									38H-4, 0	339.90	376.69	**342.45**	**342.45**	**342.45**	**342.45**	0.00
C5ACr/C5ADn	14.194									38H-6, 0	342.90	379.69	**345.17**	**345.17**	**345.17**	**345.17**	0.00
C5ADn/C5ADr	14.581									40H-1, 0	354.40	392.08	**356.44**	**356.44**	**356.44**	**356.44**	0.00
C5ADr/C5Bn.1n	14.784					39H-2, 87*	351.77	394.00	354.00	40H-2, 72	356.62	394.30	**358.45**	**358.45**	**358.45**	**358.45**	0.00
C5Bn.1n/C5Bn.1r	14.877					39H-3, 77*	353.17	395.40	355.26	40H-3, 37	357.77	395.45	**359.50**	**359.50**	**359.50**	**359.50**	0.00
C5Bn.1r/C5Bn.2n	15.032									41H-3, 40	367.30	405.59	**368.72**	**368.72**	**368.72**	**368.72**	0.00
C5Bn.2n/C5Br	15.160					40H-6, 0*	366.40	408.80	367.30	41H-5, 80	370.70	408.99	**371.81**	**371.81**	**371.81**	**371.81**	0.00

* = data from Hole U1338B not used (see text). Age column data are from Table T6 in the "Methods" chapter (Expedition 320/321 Scientists, 2010a). Core, section, interval measurements are from Table T15 in the "Site U1338" chapter (Expedition 320/321 Scientists, 2010b). CSF-A and CCSF-A depths are from Table T5 in Wilkens et al. (2013). Revised depth = CCSF-A (m)/hole growth factor (Fig. F1). Bold = shallowest and deepest depths of individual biohorizons.

Table T4. Age-depth control points (CPs) and linear sedimentation rates (LSRs), Site U1338.

CP	Biohorizons and geomagnetic chron boundaries	Age (Ma)	Depth CCSF-B (m)	LSR (m/My)	Figure
	Top Site U1338 sediment section	0.00	0.00		F3
1	C1n/C1r (Bruhnes/Matuyama)	0.781	8.98	11	F3
2	C2n/C2r.1r (Olduvai/Matuyama)	1.945	22.96	12	F3
3	C2An.3n/C2Ar (Gauss/Gilbert)	3.596	44.24	13	F3
4	Base *Asteromphalus elegans* (D)	4.2	53.11	15	F3
5	Top *Ceratolithus acutus* (N)	5.04	68.63	18	F3/F4
6	C4An/C4Ar.1r	9.098	190.60	30	F4
7	C5n.1r/C5n.2n	9.987	205.94	17	F4/F5
8	C5AAn/C5AAr	13.183	315.75	34	F5
9	C5Bn.2n/C5Br	15.160	371.81	28	F5
10	Base *Discoaster signus* (N)	15.73	384.56	22	F5
11	Base common *Sphenolithus heteromorphus* (N)	17.74	406.43	11	F5
	Hole U1338B terminal depth	18.4	413.6		

D = diatom, N = nannofossil.